Supplementary Information for "Protecting qubit coherence by spectrally engineered driving of the spin environment"

Maxime Joos[1], Dolev Bluvstein[1,2], Yuanqi Lyu[1,3], David Weld[1] and Ania Bleszynski Jayich[1*]

[1]Department of Physics, University of California, Santa Barbara, 93106, CA, USA.
[2]Department of Physics, Harvard University, Cambridge, 02138, MA, USA.
[3]Department of Physics, University of California, Berkeley, 94720, CA, USA.
[*]Corresponding author: ania@physics.ucsb.edu.

Supplementary Note 1: Definition of symbols used in this work

We summarize in Supplementary Table 1 some of the symbols used in this work.

Γ	relaxation rate of a bath spin
$\tau_c = 1/\Gamma$	bath correlation time without driving
$1/R$	correlation time of bath subject to stochastic driving
$2\Gamma_2$	inhomogeneous broadening (FWHM) of bath spins
T_2	Hahn-echo coherence time of NV

Supplementary Table 1: Symbols summary.

Supplementary Note 2: Investigated NVs

The data presented in the main text are based on the study of one nanopillar, referred to as pillar **A**. Another nanopillar (pillar **B**) was measured, showing a similar extension of NV coherence time $T_2(\Omega_{\mathrm{ss}}, \Delta\nu)$ as shown in Supplementary Fig. 1 (c) and (d). Photon coincidence measurements $g^{(2)}$ were performed on both pillars and the results are consistent with pillar **B** hosting one NV center and pillar **A** hosting 2 NV centers of the same orientation. Importantly, the same 2-bath model is necessary to fit the single NV pillar **B** confirming that the 2-bath model is not a consequence of having 2 NVs.

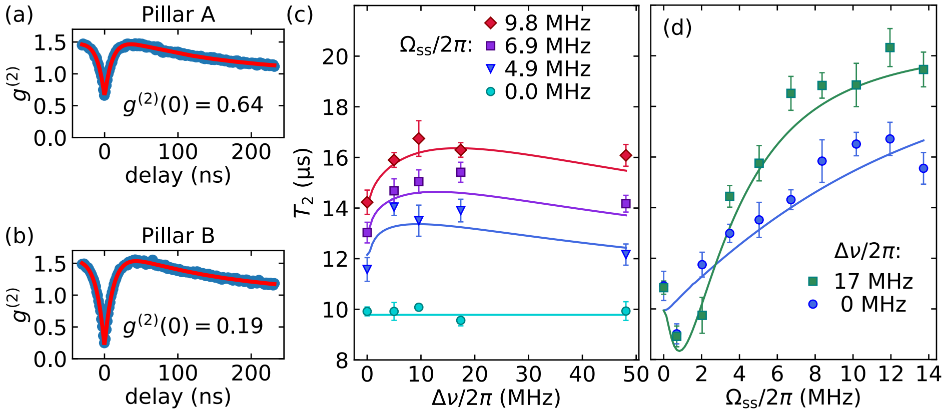

Supplementary Figure 1: **Investigated pillars**. (a) Photon coincidence measurement on pillar A. (b) Photon coincidence measurement on pillar B. (c) NV **B** T_2 as a function of $\Delta\nu$ for different bath Rabi frequencies Ω_{ss}. Stochastic drive outperforms monochromatic drive ($\Delta\nu = 0$). (d) NV **B** T_2 as a function of drive Rabi frequency Ω_{ss} for monochromatic driving $\Delta\nu = 0$ and stochastic driving with $\Delta\nu/2\pi = 17$ MHz.

Fitted baths parameters for pillars **A** and **B** can be found in Supplementary Table 2.

Supplementary Note 3: Bath model

Multiple baths

We show in Supplementary Fig. 2(a) a schematic representation of our model to simulate NV coherence. We consider up to two baths of driven electronic spins and one residual (non-driven) bath. Each bath is characterized by a correlation time τ_c, and an NV-coupling $b = \gamma B_{rms}$ where γ is the gyromagnetic ratio and B_{rms} is the root mean square of the corresponding magnetic field at

		Pillar **A**		Pillar **B**	
		Fig. 4(a)	Fig. 4(b)	Supplementary Fig. 1(a)	Supplementary Fig. 1(b)
long-lived bath	τ_c (µs)	6.4 ± 1.2	68 ± 17	5.5 ± 1.9	87 ± 37
	$b/2\pi$ (kHz)	11.6 ± 0.5	14 ± 1	25 ± 1	31 ± 3
	$2\Gamma_2$ (MHz)	4.7 ± 0.6	2.5 ± 0.4	10.1 ± 1.7	15.4 ± 2.2
short-lived bath	τ_c (µs)	0.11 ± 0.02	0.37 ± 0.05	0.05 ± 0.01	0.23 ± 0.05
	$b/2\pi$ (kHz)	54 ± 6	38 ± 3	162 ± 24	78 ± 8
	$2\Gamma_2$ (MHz)	35.8 ± 5.2	19.8 ± 3.1	40 ± 8	14.9 ± 1.6
residual bath	τ_c (µs)	12.5 ± 5.6	9.4 ± 1.8	0.75 ± 0.15	0.62 ± 0.09
	$b/2\pi$ (kHz)	2.9 ± 0.4	3.9 ± 0.3	26 ± 4	32 ± 2

Supplementary Table 2: Fitted bath parameters.

the NV location. The rf-driven baths are additionally characterized by an inhomogeneous broadening $2\Gamma_2$ which corresponds to the FWHM of the assumed Gaussian frequency distribution of the spins.

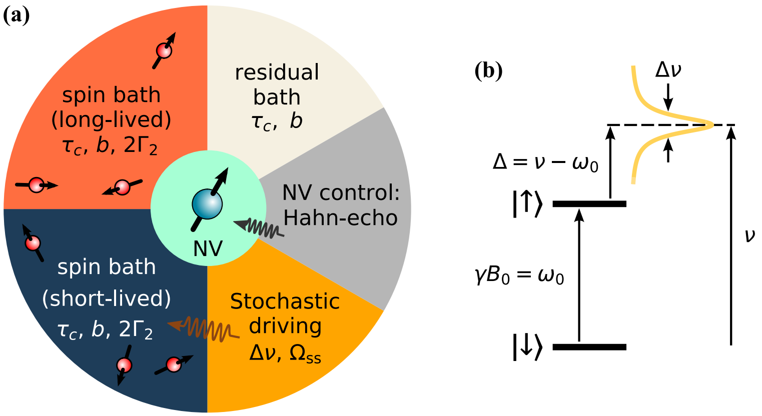

Supplementary Figure 2: **Surface-spin bath model**. **(a)** Multiple-bath model to simulate Hahn-echo decay of a shallow NV center. **(b)** Frequency diagram of a two-level system with resonance frequency ω_0 interacting with a stochastic field with carrier frequency ν and linewidth $\Delta\nu$.

We model the magnetic field of a driven bath as the sum of the fields generated by uncorrelated $g = 2$ spin-1/2 particles, where the particles are driven by a stochastic field with FWHM $\Delta\nu$ and Rabi frequency Ω_{ss}. In the next section, we consider the magnetic field radiation of a single bath spin.

Radiation of a single spin-1/2 particle

The energy level diagram for a single surface spin is shown in Supplementary Fig. 2(b). We consider here only the radiation from the longitudinal component (along z, the direction of the static field B_0) of the spin magnetic moment, involving frequencies on the order of $\Gamma, \Omega_{\mathrm{ss}}$. The transverse dynamics of the spin occur at higher frequencies that are filtered out by the Hahn-echo sequence. Therefore, we can assume that $B(t) \propto \hat{S}_z(t) \propto \sigma_z(t)$ where $\hat{S}_z$ is the z component of the spin operator and σ_z is the z Pauli matrix in the Heisenberg picture. The radiation of a single spin j is therefore fully characterized by the auto-correlation of $\sigma_z^j(t)$:

$$c_j(t) = \langle \sigma_z^j(t' + t)\sigma_z^j(t') \rangle. \tag{1}$$

By virtue of the quantum regression theorem [1], the spin correlation function in Eq. (1) is a solution of the system master equation (see section below for a derivation).

The radiated spectrum is proportional to the Fourier transform of $c_j(t)$:

$$S_j(\omega) = b_j^2 \int_{-\infty}^{+\infty} c_j(t) e^{-i\omega t} dt, \tag{2}$$

where b_j is the NV-spin-j coupling rate. In this work, we used the python package qutip for numerical calculations of $c(t)$ (qutip function *correlation_2op_1t*) and $S(\omega)$ (qutip function *spectrum*).

Total radiation and inhomogeneous broadening

In order to take into account inhomogeneous broadening of the spins, we assume that the total field at the NV location results from the contribution of n uncorrelated spins so that the total field auto-correlation is given by:

$$c(t) \propto \sum_j^n c_j(t) G(\Delta_j) \tag{3}$$

where c_j is the normalized auto-correlation function of the field due to spin j with detuning Δ_j with respect to γB_0, G is a Gaussian function centered at zero with FWHM $2\Gamma_2$.

The total spectrum associated with the driven bath is:

$$S(\omega) = b^2 \int_{-\infty}^{+\infty} c(t) e^{-i\omega t} dt, \tag{4}$$

where b is the NV-bath coupling. The spectrum is normalized to $\int_{-\infty}^{+\infty} S(\omega) d\omega / 2\pi = b^2$.

Master equation

The master equation (to be derived in this section) describing a spin-1/2 particle interacting with a partially coherent field with FWHM $\Delta\nu$ and Rabi frequency Ω_{ss} is given by ($\hbar = 1$):

$$\dot{\rho} = -i\,[H,\rho] + \frac{\Gamma}{2}\left(\mathcal{D}[\sigma_-]\rho + \mathcal{D}[\sigma_+]\rho\right) + \frac{\Delta\nu}{4}\mathcal{D}[\sigma_z]\rho \tag{5}$$

where $\mathcal{D}[c]\rho = c\rho c^\dagger - \frac{1}{2}(c^\dagger c\rho + \rho c^\dagger c)$ is the Lindblad superoperator, i is the imaginary unit, $H = -\Delta\sigma_+\sigma_- + \frac{\Omega_{\mathrm{ss}}}{2}(\sigma_+ + \sigma_-)$ is the closed system Hamiltonian in the rotating-frame approximation with $\Delta = \nu - \omega_0$, $\sigma_+ = |{\uparrow}\rangle\langle{\downarrow}|$, $\sigma_- = |{\downarrow}\rangle\langle{\uparrow}|$, and $\sigma_z = \sigma_+\sigma_- - \sigma_-\sigma_+$. Γ is the relaxation rate of the spin system. Note that at room temperature, $k_B T \gg \hbar\omega_0$, so we are dealing with bidirectional transitions: $\Gamma_{\uparrow\to\downarrow} = \Gamma_{\downarrow\to\uparrow} = \Gamma/2$.

The master equation (5) is valid for the average density matrix elements $\langle\rho_{ij}\rangle = \langle\langle i|\,\rho\,|j\rangle\rangle$ and $i,j = \{\uparrow,\downarrow\}$ of a single spin-1/2 system. The outer bracket denotes a classical ensemble average over the statistics of the driving field. The frequency diagram of a two-level system interacting with a stochastic field in shown in Supplementary Fig. 2(b).

To derive Eq. (5), we start from the time-dependent Hamiltonian for the spin-1/2 system interacting with a stochastic field:

$$H(t) = \frac{\omega_0}{2}\sigma_z + \frac{\Omega_{\mathrm{ss}}}{2}\left[\sigma_x\cos(\nu t - \phi(t)) + \sigma_y\sin(\nu t - \phi(t))\right], \tag{6}$$

where $\sigma_{x,y,z}$ are the Pauli matrices, $\hbar\omega_0$ is the energy splitting of the 2-level system, Ω_{ss} the Rabi frequency and $\phi(t)$ the stochastic phase trace. The master equation of the Lindblad form reads:

$$\dot{\rho} = -i\,[H(t),\rho] + \frac{\Gamma}{2}\mathcal{D}[\sigma_-]\rho + \frac{\Gamma}{2}\mathcal{D}[\sigma_+]\rho, \tag{7}$$

leading to the following system of differential equations:

$$\begin{aligned}
\dot{\rho}_{\uparrow\uparrow} &= \frac{i\Omega_{\mathrm{ss}}}{2}\left[e^{i(\nu t-\phi(t))}\rho_{\uparrow\downarrow} - e^{-i(\nu t-\phi(t))}\rho_{\downarrow\uparrow}\right] - \frac{\Gamma}{2}\rho_{\uparrow\uparrow} + \frac{\Gamma}{2}\rho_{\downarrow\downarrow}\\
\dot{\rho}_{\downarrow\downarrow} &= \frac{i\Omega_{\mathrm{ss}}}{2}\left[e^{-i(\nu t-\phi(t))}\rho_{\downarrow\uparrow} - e^{i(\nu t-\phi(t))}\rho_{\uparrow\downarrow}\right] + \frac{\Gamma}{2}\rho_{\uparrow\uparrow} - \frac{\Gamma}{2}\rho_{\downarrow\downarrow}\\
\dot{\rho}_{\uparrow\downarrow} &= -i\omega_0\rho_{\uparrow\downarrow} - \frac{\Gamma}{2}\rho_{\uparrow\downarrow} + \frac{i\Omega_{\mathrm{ss}}}{2}e^{-i(\nu t-\phi(t))}(\rho_{\uparrow\uparrow} - \rho_{\downarrow\downarrow})\\
\dot{\rho}_{\downarrow\uparrow} &= i\omega_0\rho_{\downarrow\uparrow} - \frac{\Gamma}{2}\rho_{\downarrow\uparrow} + \frac{i\Omega_{\mathrm{ss}}}{2}e^{i(\nu t-\phi(t))}(\rho_{\downarrow\downarrow} - \rho_{\uparrow\uparrow}).
\end{aligned} \tag{8}$$

We now perform the rotating-frame transformations:

$$\begin{aligned}
\rho_{\uparrow\uparrow} &= \widetilde{\rho}_{\uparrow\uparrow}\\
\rho_{\downarrow\downarrow} &= \widetilde{\rho}_{\downarrow\downarrow}\\
\rho_{\uparrow\downarrow} &= \widetilde{\rho}_{\uparrow\downarrow}e^{-i(\nu t-\phi(t))}\\
\rho_{\downarrow\uparrow} &= \widetilde{\rho}_{\downarrow\uparrow}e^{i(\nu t-\phi(t))},
\end{aligned} \tag{9}$$

and obtain the following simplified equations:

$$\begin{aligned}
\dot{\widetilde{\rho}}_{\uparrow\uparrow} &= \frac{i\Omega_{\mathrm{ss}}}{2}(\widetilde{\rho}_{\uparrow\downarrow} - \widetilde{\rho}_{\downarrow\uparrow}) - \frac{\Gamma}{2}(\widetilde{\rho}_{\uparrow\uparrow} - \widetilde{\rho}_{\downarrow\downarrow}) \\
\dot{\widetilde{\rho}}_{\downarrow\downarrow} &= \frac{i\Omega_{\mathrm{ss}}}{2}(\widetilde{\rho}_{\downarrow\uparrow} - \widetilde{\rho}_{\uparrow\downarrow}) + \frac{\Gamma}{2}(\widetilde{\rho}_{\uparrow\uparrow} - \widetilde{\rho}_{\downarrow\downarrow}) \\
\dot{\widetilde{\rho}}_{\uparrow\downarrow} &= \left[i(\Delta - \dot{\phi}(t)) - \frac{\Gamma}{2}\right]\widetilde{\rho}_{\uparrow\downarrow} + \frac{i\Omega_{\mathrm{ss}}}{2}(\widetilde{\rho}_{\uparrow\uparrow} - \widetilde{\rho}_{\downarrow\downarrow}) \\
\dot{\widetilde{\rho}}_{\downarrow\uparrow} &= \left[-i(\Delta - \dot{\phi}(t)) - \frac{\Gamma}{2}\right]\widetilde{\rho}_{\downarrow\uparrow} + \frac{i\Omega_{\mathrm{ss}}}{2}(\widetilde{\rho}_{\downarrow\downarrow} - \widetilde{\rho}_{\uparrow\uparrow}),
\end{aligned} \tag{10}$$

where $\Delta = \nu - \omega_0$ is the rf field detuning. Put in this form, the equations highlight the phase diffusion model [2] used to generate the finite bandwidth of the drive: the phase derivative $\dot{\phi}(t)$ is equivalent to the time-dependent detuning of the rf field.

The system of equations (10) is general and valid for an arbitrary phase trace $\phi(t)$. In this work, we choose specific statistical properties for $\dot{\phi}(t)$ which enables to derive simple equations for the average density matrix elements. We assume that $\dot{\phi}(t)$ is a random, stationary and Gaussian process with zero average $\langle\dot{\phi}(t)\rangle = 0$ and mean square correlation $\langle\dot{\phi}(t)\dot{\phi}(t')\rangle = \Delta\nu\ \delta(t-t')$. Using the results for multiplicative stochastic processes [3], the average value of (10) becomes:

$$\begin{aligned}
\langle\dot{\widetilde{\rho}}_{\uparrow\uparrow}\rangle &= \frac{i\Omega_{\mathrm{ss}}}{2}(\langle\widetilde{\rho}_{\uparrow\downarrow}\rangle - \langle\widetilde{\rho}_{\downarrow\uparrow}\rangle) - \frac{\Gamma}{2}(\langle\widetilde{\rho}_{\uparrow\uparrow}\rangle - \langle\widetilde{\rho}_{\downarrow\downarrow}\rangle) \\
\langle\dot{\widetilde{\rho}}_{\downarrow\downarrow}\rangle &= \frac{i\Omega_{\mathrm{ss}}}{2}(\langle\widetilde{\rho}_{\downarrow\uparrow}\rangle - \langle\widetilde{\rho}_{\uparrow\downarrow}\rangle) + \frac{\Gamma}{2}(\langle\widetilde{\rho}_{\uparrow\uparrow}\rangle - \langle\widetilde{\rho}_{\downarrow\downarrow}\rangle) \\
\langle\dot{\widetilde{\rho}}_{\uparrow\downarrow}\rangle &= \left[i\Delta - \frac{\Delta\nu}{2} - \frac{\Gamma}{2}\right]\langle\widetilde{\rho}_{\uparrow\downarrow}\rangle + \frac{i\Omega_{\mathrm{ss}}}{2}(\langle\widetilde{\rho}_{\uparrow\uparrow}\rangle - \langle\widetilde{\rho}_{\downarrow\downarrow}\rangle) \\
\langle\dot{\widetilde{\rho}}_{\downarrow\uparrow}\rangle &= \left[-i\Delta - \frac{\Delta\nu}{2} - \frac{\Gamma}{2}\right]\langle\widetilde{\rho}_{\downarrow\uparrow}\rangle + \frac{i\Omega_{\mathrm{ss}}}{2}(\langle\widetilde{\rho}_{\downarrow\downarrow}\rangle - \langle\widetilde{\rho}_{\uparrow\uparrow}\rangle),
\end{aligned} \tag{11}$$

which can be recast in the Lindblad form (5).

Adiabatic approximation

It is possible to find approximations of (11) by adiabatic elimination, i.e by setting $\langle\dot{\widetilde{\rho}}_{\uparrow\downarrow}\rangle = \langle\dot{\widetilde{\rho}}_{\downarrow\uparrow}\rangle = 0$, which is valid in the limit $|2i\Delta - \Delta\nu - \Gamma| \gg \Omega_{\mathrm{ss}}$. By substituting the adiabatic solutions:

$$\begin{aligned}
\langle\widetilde{\rho}_{\uparrow\downarrow}\rangle &= \frac{i\Omega_{\mathrm{ss}}}{2}(\langle\widetilde{\rho}_{\uparrow\uparrow}\rangle - \langle\widetilde{\rho}_{\downarrow\downarrow}\rangle)\frac{1}{-i\Delta + \delta + \frac{\Gamma}{2}} \\
\langle\widetilde{\rho}_{\downarrow\uparrow}\rangle &= \frac{i\Omega_{\mathrm{ss}}}{2}(\langle\widetilde{\rho}_{\downarrow\downarrow}\rangle - \langle\widetilde{\rho}_{\uparrow\uparrow}\rangle)\frac{1}{i\Delta + \delta + \frac{\Gamma}{2}}
\end{aligned} \tag{12}$$

into (11), we find the rate equations:

$$\begin{aligned}\langle\dot{\widetilde{\rho}}_{\uparrow\uparrow}\rangle &= -\frac{R}{2}(\langle\widetilde{\rho}_{\uparrow\uparrow}\rangle - \langle\widetilde{\rho}_{\downarrow\downarrow}\rangle)\\ \langle\dot{\widetilde{\rho}}_{\downarrow\downarrow}\rangle &= \frac{R}{2}(\langle\widetilde{\rho}_{\uparrow\uparrow}\rangle - \langle\widetilde{\rho}_{\downarrow\downarrow}\rangle)\end{aligned} \tag{13}$$

where R is the effective relaxation rate of the spin system under stochastic drive and is given by:

$$R = \Gamma + \frac{\Omega_{ss}^2}{2}\frac{\Delta\nu + \Gamma}{\Delta^2 + \left(\frac{\Delta\nu+\Gamma}{2}\right)^2}, \tag{14}$$

which reduces to Eq. (3) of the main text in the case of $\Delta = 0$ and $\Delta\nu \gg \Gamma$.

Analysis of DEER sequence

DEER spectrum

The DEER spectrum (Fig. 3(b) of the main text) can be well understood by assuming inhomogeneous broadening of the surface spins. The response of a single spin, initially in $|\downarrow\rangle$, to a single-tone pulse of duration $t = \pi/\Omega_{\mathrm{ss}}$ (π-pulse) is given by the generalized Rabi formula:

$$\rho_{\uparrow\uparrow}(\Delta) = \frac{\Omega_{\mathrm{ss}}^2}{\Delta^2 + \Omega_{\mathrm{ss}}^2}\sin^2\left(\frac{\sqrt{\Delta^2 + \Omega_{\mathrm{ss}}^2}}{\Omega_{\mathrm{ss}}}\frac{\pi}{2}\right), \tag{15}$$

where $\Delta = \nu - \omega_0$, and Ω_{ss} is the Rabi frequency.

The DEER resonance spectrum is modeled as the convolution of Eq. (15) with a Gaussian function (with FWHM $2\Gamma_2$ as a fitting parameter) describing the frequency distribution of the inhomogeneous spins.

Bath correlations from DEER

We describe in this section the model employed to fit the DEER signal plotted in Fig. 3(c) and (d) of the main text. The NV coherence is given by [4]:

$$C(t_{ss}) = ae^{-\langle(\delta\Phi)^2\rangle/2}, \tag{16}$$

where a is the T_2-limited initial NV coherence and $\delta\Phi$ is the random phase accumulated during one realisation of the DEER sequence of Fig. 3(a) of the main text:

$$
\begin{aligned}
\langle(\delta\Phi)^2\rangle &= \gamma^2 \left\langle \left[\int_0^{\tau/2} B(t)dt - \int_{\tau/2}^{\tau} B(t)dt \right]^2 \right\rangle \\
&\approx \gamma^2 \left\langle [\frac{\tau}{2} B((\tau - t_{ss})/2) - \frac{\tau}{2} B(\tau + t_{ss})/2)]^2 \right\rangle \\
&\approx \frac{\gamma^2\tau^2}{2} B_{rms}^2 [1 - c(t_{ss})] \\
&\approx \frac{b^2\tau^2}{2} [1 - c(t_{ss})]
\end{aligned}
\tag{17}
$$

where b is the NV-bath coupling rate, τ the sequence duration, t_{ss} is the DEER pulse duration, and $c(t)$ is the normalized correlation function of the field. In order to derive line 2 of Eq. (17), we assume a quasistatic bath so that $B(t)$ is approximately constant over the integration range. Therefore, the measured NV coherence is fitted with the model:

$$
C(t_{ss}) = ae^{-\frac{b^2\tau^2}{4}[1-c(t_{ss})]}, \tag{18}
$$

where $c(t_{ss})$ has the fitting parameters τ_c, Ω_{ss} and $2\Gamma_2$. In the broad excitation limit $\Delta\nu \gg \Omega_{\mathrm{ss}}, \Gamma$, $c(t_{ss})$ is an exponential decay with rate $R = \Gamma + 2\frac{\Omega_{\mathrm{ss}}^2}{\Delta\nu}$.

The spectrum in Fig. 3(d) of the main text is the Fourier transform of the fitted function $c(t_{ss})$ after proper symmetrization:

$$
S_{norm}(\omega) = \int_{-\infty}^{+\infty} c(t_{ss}) e^{-i\omega t_{ss}} dt_{ss}. \tag{19}
$$

Two-bath model

The experimental results presented in Fig. 4 of the main text are well modelled by assuming contributions from two baths of electronic spins; this simple model has been applied in previous experiments studying surface spin-induced decoherence of NV centers [5, 6] with good agreement.

To illustrate the benefits of considering two baths, we show in Supplementary Fig. 3 the fitting results for different bath models. Supplementary Fig. 3(a) corresponds to fitting a model of two baths with a long and short correlation times. Supplementary Fig. 3(b) corresponds to fitting a model of one bath with a short ($\tau_c \lesssim 1\,\mu\mathrm{s}$) correlation time; the short correlated bath model does not account for the coherence dip observed at low driving powers. Supplementary Fig. 3(c) corresponds to fitting a model of one bath with a long ($\tau_c \gg 1\,\mu\mathrm{s}$) correlation time; the long correlated bath model qualitatively accounts for the coherence dip but does not quantitatively fit the data.

Our measurements are compatible with the presence of two baths with distinct correlation times and inhomogeneous broadenings. One possible future

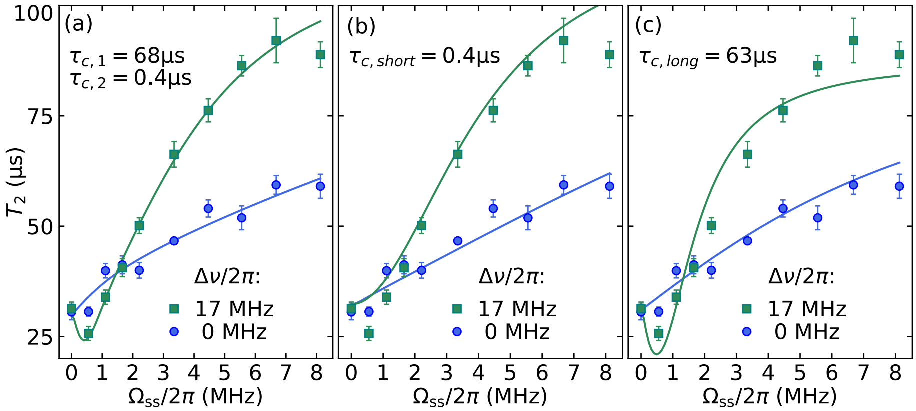

Supplementary Figure 3: **Fitting with a multiple bath model**. **(a)** Assuming two surface-spin baths with distinct correlation times. **(b)** Assuming a short correlation time for the surface-spin bath. The model does not account for the coherence dip. **(c)** Assuming a long correlation time for the surface-spin bath. The model does not fit the data as well as the two-bath model.

avenue in order to further improve NV-bath decoupling is to cover these two baths with appropriately-shaped drives.

Supplementary Note 4: Stochastic driving as a probe of the correlation time of the bath

Figure 4(b) of the main text shows a non monotonic increase of the coherence extension under stochastic driving. This feature limits the performance of stochastic driving at low powers, but is also an interesting signature of the bath correlation time.

We derive below the condition under which stochastic driving is beneficial for the extension of coherence. We depict in Supplementary Fig. 4 the typical noise spectral densities in the absence of driving (Lorentzian with HWHM Γ) and in the case of stochastic driving (Lorentzian with HWHM R). We also show a Hahn-echo filter function that peaks at an angular frequency $\omega_{NV} \sim 2\pi/T_2$, where T_2 is the NV coherence time. ω_{lim} is the angular frequency at which the spectral densities intersect. Stochastic driving reduces the overlap integral under the condition that $\omega_{lim} > \omega_{NV}$.

The undriven spectral density is proportional to $\Gamma/(\Gamma^2+\omega^2)$ whereas under broad stochastic driving, the spectral density is proportional to $R/(R^2+\omega^2)$. By equating the two spectral densities and solving for ω, we find $\omega_{lim} = \sqrt{\Gamma R}$. Hence, stochastic driving improves coherence if:

$$\sqrt{\Gamma\left(\Gamma + 2\frac{\Omega_{\rm ss}^2}{\Delta\nu}\right)} > 2\pi/T_2. \qquad (20)$$

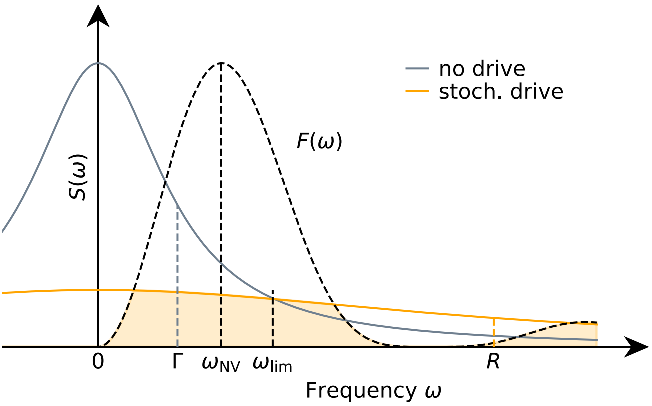

Supplementary Figure 4: **Signature of the bath correlation time under stochastic driving**. A minimum driving Rabi frequency is required for stochastic driving to induce a reduction of the overlap integral $\int d\omega S(\omega)F(\tau,\omega)$.

Therefore, for a given broadening $\Delta\nu$, a minimum driving power is necessary for stochastic driving to be beneficial.

Equation (20) can also be used to estimate the correlation time of the bath. Knowing the bare T_2 of the NV and the Rabi frequency Ω_{ss} at which stochastic driving starts to be beneficial (as extracted from Fig. 4.(b) of the main text), we can solve (20) for Γ. In our case, $T_2 = 33.1\,\mu\mathrm{s}$, and stochastic driving starts to be beneficial at $\Omega_{\mathrm{ss}}/2\pi \sim 1$ MHz, leading to an estimated bath correlation time $\tau_c = 1/\Gamma \sim 21\,\mu\mathrm{s}$ in accordance with the correlation time of long-lived species extracted from the full model fit.

Supplementary Note 5: Gaussian-shaped driving spectrum

In this section, we report on driving with a Gaussian-shaped spectrum. Supplementary Fig. 5(a) shows the measured increase of coherence when a monochromatic, Lorentzian ($\Delta\nu/2\pi = 17.4\,\mathrm{MHz}$) and Gaussian ($\Delta\nu/2\pi = 18.6\,\mathrm{MHz}$) spectrum is used with the same driving power.

For intermediate driving powers ($\Omega_{\mathrm{ss}}/2\pi \sim 1.5\,\mathrm{MHz}$), Gaussian driving extends coherence more efficiently than Lorentzian and monochromatic driving. This observation, corroborated by numerical simulations (Supplementary Fig. 5(b)), suggests that more sophisticated driving schemes could be advantageous.

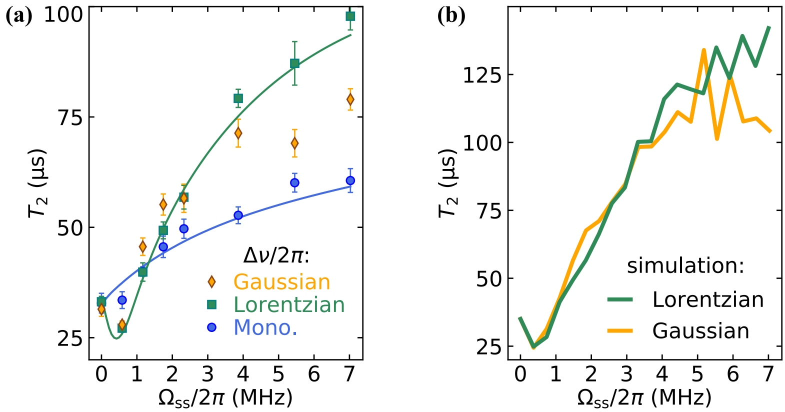

Supplementary Figure 5: **Coherence increase by driving with a Gaussian-shaped spectrum**. In a specific range of driving Rabi frequencies around $\Omega_{ss}/2\pi = 1.5\,\text{MHz}$, the measured NV coherence is longer for Gaussian-shaped than for a Lorentzian-shaped spectrum, as evidenced by data (a) and numerical simulation (b).

Supplementary Note 6: Effect of bath driving on the stretch exponent

The stretch exponent n used in this work to fit to Hahn-echo decays ($\propto \exp(-(t/T_2)^n)$) depends on the shape of the noise spectral density and therefore depends on the bath driving parameters. We show in Supplementary Fig. 6(a) the extracted stretch exponent n as a function of the drive Rabi frequency for monochromatic and stochastic driving using the same experimental data as for Fig. 4(b) of the main text. We note that the initial sharp decrease of stretch exponent from $n \sim 1.6$ to $n \sim 1$ observed with stochastic driving ($\Delta\nu/2\pi = 17$ MHz) is compatible with a "flattening" of the noise spectrum (expected stretch exponent for "flat" white noise is $n = 1$). The subsequent increase of the stretch exponent for increasing Ω_{ss} can be understood as decoupling the NV from surface spins resulting in residual noise sources with Lorentzian spectral densities dominating the NV decoherence and therefore leading to a larger stretch exponent of the Hahn-echo decay.

We discuss now the covariance of fit parameters T_2 and n and the potential impact on the estimate of the parameter uncertainties. We illustrate in Supplementary Fig. 6(b) the weak correlation between parameters T_2 and n by fitting the same experimental decay with two distinct stretch exponent. Fixing the stretch exponent parameter does not affect considerably the extracted T_2. Therefore, fit parameter error bars (corresponding to $\pm$ one standard deviation assuming no covariance between parameters) are a reasonable estimate of the parameter uncertainties.

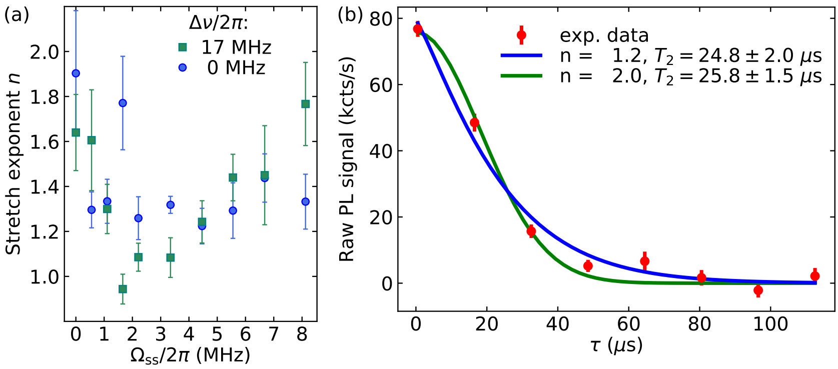

Supplementary Figure 6: **Stretch exponent parameter**. (a) Stretch exponent as a function of drive Rabi frequency Ω_{ss} for monochromatic driving $\Delta\nu = 0$ and stochastic driving with $\Delta\nu/2\pi = 17$ MHz. We use the same experimental data as for Fig. 4(b) of the main text. (b) Fitting experimental data with two distinct values of n gives similar T_2 illustrating the small correlations between those fit parameters. Data at the origin of this plot corresponds to $\Delta\nu = 17$ MHz, $\Omega_{ss}/2\pi = 0.56$ MHz.

Supplementary References

[1] Gardiner, C.W & Zoller, P. Quantum Noise (Springer-Verlag Berlin Heidelberg, 2000).

[2] Agarwal, G.S. Exact solution for the influence of laser temporal fluctuations on resonance fluorescence. Phys. Rev. Lett. **37**, 1383-1386 (1976).

[3] Fox, R.F. Contributions to the theory of multiplicative stochastic processes. J. Math. Phys. **13**(8), 1196-1207 (1972).

[4] Mamin, H.J. & Sherwood, M.H. & Rugar, D. Detecting external electron spins using nitrogen-vacancy centers. Phys. Rev. B **86**, 195422 (2012).

[5] Myers, B.A. *et al.* Probing surface noise with depth-calibrated spins in diamond. Phys. Rev. Lett. **113**(2), 027602 (2014).

[6] Romach, Y. *et al.* Spectroscopy of surface-induced noise using shallow spins in diamond. Phys. Rev. Lett. **114**, 017601 (2015).